buildings

MDPI

Article

Durability Analysis of Bamboo Fiber Recycled Concrete Subjected to Wet and Dry Sulfate Cycling

Chuheng Zhong [1,2,3], Ronglian Sun [1], Jinzhi Zhou [4,*] and Shuai Wang [5]

[1] School of Civil Engineering, Architecture and Environment, Hubei University of Technology, Wuhan 430068, China
[2] Key Laboratory of Intelligent Health Perception and Ecological Restoration of River and Lake, Ministry of Education, Hubei University of Technology, Wuhan 430068, China
[3] China Railway Major Bridge Engineering Group Co., Ltd., Wuhan 430050, China
[4] Engineering and Technology College, Hubei University of Technology, Wuhan 430068, China
[5] Zhongcai India Chemical Building Material Private Limited, Hangzhou 310018, China
* Correspondence: zhoujinzhi@hbut.edu.cn

Abstract

This study investigates the durability performance of bamboo fiber recycled aggregate concrete (BFRAC) in a sulfate attack environment by simulating harsh conditions through dry–wet cyclic tests. It compares the sulfate attack resistance of steel fiber recycled aggregate concrete (SFRAC) and BFRAC, analyzing their durability performance. The experiments were designed with bamboo fiber admixtures (by volume) of 1%, 1.5%, and 2%, using a 5% Na_2SO_4 solution for dry–wet cycling. The tests evaluated the mass loss rate, microstructure evolution, compressive strength corrosion resistance coefficient, split tensile strength, and dynamic modulus at cycles 0, 30, 60, 90, and 120. A damage model was established to predict the concrete's damage life. The results showed that as the number of wet and dry cycles increased, the specimens developed cracks, mortar detachment, and fiber rusting on the surface. The mass loss initially increased and then decreased, while the relative dynamic modulus of elasticity and compressive strength exhibited a trend of increasing followed by a decrease. Bamboo fiber concrete demonstrated better durability in terms of compressive strength and splitting tensile strength. Among the BFRAC specimens, those with a 1.5% bamboo fiber admixture had the longest predicted service life, as determined by the Weibull distribution model.

Keywords: bamboo fiber; recycled coarse aggregate; sulfate erosion; dry–wet cycling

Check for updates

Academic Editor: Salvatore Verre

Received: 29 December 2025
Revised: 23 January 2026
Accepted: 2 March 2026
Published: 6 March 2026

Copyright: © 2026 by the authors. Licensee MDPI, Basel, Switzerland. This article is an open access article distributed under the terms and conditions of the Creative Commons Attribution (CC BY) license.

1. Introduction

As construction waste continues to increase annually, the use of Recycled Aggregate (RA) has become a crucial grand strategy to alleviate the scarcity of natural aggregate resources and reduce environmental burdens. A large number of techniques in the construction industry deal with the mixture, reinforcement and use of concrete and related materials [1]. The widespread application of recycled aggregate concrete not only minimizes the consumption of natural aggregates in construction but also lessens the environmental impact associated with their extraction [2], thereby promoting a harmonious balance between socio-economic and environmental development [3,4]. However, Recycled Aggregate Coarse (RAC) concrete contains a significant amount of aged mortar on its surface, and its loose structure, along with multi-layer interfacial transition zones, results in defects in its mechanical properties [5]. The porosity of recycled aggregate concrete

is significantly higher than that of ordinary concrete. Sulfate ions penetrate the matrix through the pores of recycled aggregate concrete, which severely impacts its structural mechanical properties and durability [6]. To further advance the recycling of recycled aggregates, enhance the structural performance of recycled concrete, and support sustainable building development and green transformation, studying measures to improve the overall performance of recycled concrete is of great significance. Current studies predominantly focus on conventional synthetic fibers such as steel fibers and polypropylene fibers, and most employ a single erosion mode involving static sulfate immersion. Regarding the introduction of eco-friendly fibers like natural bamboo fibers, the existing literature only addresses mechanical properties under dry or standard aqueous conditions, lacking systematic investigation under cyclic sulfate dry–wet exposure. Furthermore, no reports have compared the mechanisms of damage evolution in recycled concrete caused by bamboo fibers versus steel fibers during sulfate erosion. These research gaps provide the necessity and foundation for this study.

China's vast territory is characterized by a widespread distribution of sulfates. The erosion of sulfates leads to the formation of gypsum and calcium aluminate through chemical reactions, which can cause concrete expansion, cracking, strength loss, spalling, and ultimately result in structural failure [7]. Dry–wet cycling is a key factor that induces significant structural damage. Therefore, studying the impact of sulfate dry–wet cycling on the performance of recycled aggregate concrete holds practical value. Yu Hong fa et al. [8] found that in the western salt lakes area, concrete located more than 30 cm above the ground in regions subject to wet–dry cycling experiences significant salt crystallization and erosion damage. Ordinary concrete exposed to salt lake brine and wet–dry cycling environments undergoes severe salt crystallization damage after approximately 2–3 years, with a destruction rate that is faster than chemical corrosion. Sulfate erosion is a significant durability issue for recycled concrete structures and sufficient attention must be paid to its effects [9,10]. In this context, both domestic and international researchers have conducted numerous studies on this subject.

Zhang et al. [11] demonstrated in their study that, under the combined influence of sulfate erosion and wet/dry cycles, the sulfate ion concentration in recycled aggregate concrete (RAC) was higher than that in conventional concrete (C) at the same erosion depth. All types of interfacial transition zones (ITZs) in the RAC experienced erosion reactions, though the major erosion products varied across different ITZs. Old mortar's resistance to a sulfate attack was significantly lower than that of new mortar under long-term erosive conditions and its ITZ performance was also poorer, further exacerbating the erosive deterioration of the RAC. Xie et al. [12] subjected RAC to wet and dry cycling tests with complete and partial immersion in 0% and 5% sodium sulfate solutions, respectively, for 40 weeks. The results showed that RAC exhibited significant differences in damage behavior under different exposure conditions. Feng et al. [13] concluded that the primary cause of expansion, cracking, and spalling in concrete specimens after sulfate attack is the expansion stresses generated by caliche. Additionally, the formation of calcite and gypsum requires calcium sources, which can be supplied through the dissolution of calcium hydroxide (portlandite) or C-S-H. Calcium C-S-H dissolution due to a sulfate attack also leads to the degradation of concrete's properties due to the dominant contribution of C-S-H to concrete strength [14]. The study by Ben Yi Xie [15] showed that the compressive strength, dynamic elastic modulus, and mass of alkali slag recycled concrete continued to increase with erosion age under sulfate wet/dry cycling conditions, without exhibiting a decreasing trend. In contrast, the compressive strength, dynamic elastic modulus, and mass of ordinary recycled concrete initially increased before decreasing with erosion age. Karthikeyan et al. [16] tested the compressive strength, splitting tensile strength and

flexural strength of bamboo fiber concrete in different proportions. The results show that the strength of bamboo fiber-reinforced concrete peaks at 2% fiber addition and decreases slightly beyond this percentage. Flexural strength tests also showed a similar trend. A large number of scholars have strongly contributed to the depth and breadth of research on the sulfate erosion resistance of recycled concrete.

Bamboo fiber, a green, environmentally friendly, and rust-resistant natural material, has gradually gained attention in recent years [17]. While studies have demonstrated that bamboo fiber can effectively enhance the mechanical properties and durability of concrete, systematic research on Bamboo Fiber-Reinforced Concrete (BFRAC) remains limited. In particular, the sulfate durability of BFRAC has not yet been thoroughly investigated. This study investigates the changes in the apparent morphology, mass loss rate, relative modulus of elasticity, compressive strength, and split tensile strength of recycled concrete under the combined effects of wet/dry cycles and sulfate erosion. It also reveals the damage deterioration mechanism of recycled concrete under composite erosion from a microscopic perspective using scanning electron microscopy (SEM) [18]. This study analyzes the damage mechanism of recycled concrete under the combined effects of dry–wet cycling and sulfate erosion, as well as the interaction between these two factors. A durability damage model is then established to account for the dual action of dry–wet cycling and sulfate erosion. Finally, the lifespan of the concrete is predicted using Weibull theory.

2. Material and Sample Preparation

2.1. Raw Material

Coarse aggregate comprises natural and recycled coarse aggregates, with a particle size range of 5–20 mm and is a continuously graded aggregate. Fine aggregate was sourced from manufactured sand provided by a commercial concrete mixing station of China Construction. The cementitious material consists of a blend of P.O. 42.5-grade ordinary Portland cement and grade II fly ash. P.O. A 42.5-grade ordinary Portland cement (OPC) from Zhong jian Commercial Concrete Mixing Station was used as the binder, and grade II fly ash (FA) from the same source was employed as the supplementary cementitious material. A polycarboxylic acid high-efficiency water-reducing agent, purchased from Shanxi Feike New Material Science and Technology Co. in Yuncheng, China, was used to reduce water content. Sodium sulfate (Na_2SO_4), with a relative molecular mass of 142.04, was also included. Drinking water was used as the mixing water, and the fibers consisted of ordinary steel fibers and bamboo fibers. The fiber morphology is shown in Figure 1, and the fiber properties are listed in Table 1.



(**a**) BF (**b**) SF

Figure 1. Fiber morphology.

Table 1. Fiber properties.

Fiber Type	Lengths (mm)	Diameter/Width (mm)	Densities (g/cm^3)	Price of Item (¥/kg)	Tensile Strength (MPa)	Modulus of Elasticity (GPa)
Steel fiber	40	2	7.85	6.5	380	180
Bamboo fiber	20, 40, 60	2	0.68	12	150	20

2.2. Mixing Ratio Design and Procedure

This study is based on C45 normal concrete with a water-to-cementitious material ratio of 0.42 and a total cement content of 401 kg/m^3. The recycled aggregate content was replaced by 20%; this study selected a 20% recycled aggregate replacement rate based on preliminary pre-experimental results—when the replacement rate exceeds 20%, the initial compressive strength of recycled concrete shows a significant decline. Furthermore, in line with the consensus in the existing literature, 20% is a commonly used engineering dosage that balances recycled aggregate utilization and concrete mechanical properties, and the fly ash substitution rate was also 20%. The selection of a 20% fly ash content primarily references the Technical Specification for Fly Ash Concrete Application and multiple related studies. This dosage effectively optimizes the pore structure of recycled concrete, reduces matrix porosity, and thereby enhances its resistance to sulfate attacks. Steel fibers were incorporated at 1%, 1.5%, and 2%, while bamboo fibers were added at 1%, 1.5%, and 2% (bamboo fibers were soaked in deionized water for 24 h to ensure full swelling and minimize water absorption during mixing). A liquid-to-solid ratio of 10:1 was used (1000 mL deionized water per 100 g bamboo fiber) to guarantee complete submersion and sufficient moisture for swelling. After soaking, fibers were removed and dried in a 40 °C oven for 30 min or gently pressed with industrial filter cloth until no free water remained on the fiber surface (quality control target: fiber surface dry at saturation). This prevents excess moisture from entering the mixing system. In total, eight different mixtures were formulated. C represents normal concrete made with entirely natural coarse aggregate as the control group. RAC refers to recycled concrete produced using recycled coarse aggregate without any treatment, with the RAC substitution rate being the same as stated above. SF stands for steel fibers, BF denotes bamboo fibers, and the numbers correspond to the fiber admixture percentages. The mix proportions for the different mixtures are presented in Table 2.

Table 2. Test ratios (kg/m^3).

Mix	OPC	FA	NCA	RCA	NFA	SF	BF	Water	SP
C	321	80	1198	0	631	0	0	169	2
RAC	321	80	959	240	631	0	0	169	2
1%SFRAC	321	80	959	240	631	78.5	0	169	2
1.5%SFRAC	321	80	959	240	631	117.75	0	169	2
2%SFRAC	321	80	959	240	631	157	0	169	2
1%BFRAC	321	80	959	240	631	0	7.5	169	2
1.5%BFRAC	321	80	959	240	631	0	11.25	169	2
2%BFRAC	321	80	959	240	631	0	15	169	2

Concrete specimens were prepared by calculating the test dosage of recycled concrete based on the mix ratios in Table 2. The specific process is illustrated in Figure 2. Two sizes of specimens were prepared: 100 mm × 100 mm × 100 mm and 100 mm × 100 mm × 400 mm. After molding, the specimens were demolded 48 h later and cured under standard conditions (20 °C ± 2 °C, relative humidity greater than 95%) for 28 days. The production and curing of concrete specimens were carried out in accordance with the

provisions outlined in the Standard for Test Methods of Physical and Mechanical Properties of Concrete (GB/T 50081-2019) [19].



Figure 2. Detailed procedure for preparing concrete test specimens.

3. Tests and Test Methods

Sulfate dry–wet cycle tests are crucial for studying the performance of concrete in saline and alkaline environments. The test procedure was developed in accordance with the provisions outlined in the GB/T 50082-2009 Standard for Long-Term Performance and Durability Test Methods for Ordinary Concrete. The LSY-18 sulfate dry–wet cycle apparatus was used to conduct the test, as shown in Figure 3. Three specimens were taken from each group after curing, it was observed whether the surface of the specimens met the requirements, the moisture and impurities on the surface of the specimens were dried, and they were set aside for later use. The specimens were dried in an oven at 80 °C for 48 h and then placed in a dry environment to cool to room temperature. This temperature was chosen to simulate the extreme thermal conditions experienced by concrete structures in hot summer regions during alternating wet and dry cycles. It also complies with the accelerated drying requirements specified in the Standard Test Methods for the Long-Term Performance and Durability of Ordinary Concrete. This approach significantly shortens the test cycle and has been confirmed by multiple studies to effectively reflect the erosion damage patterns observed in real-world environments. The initial mass of the specimen was weighed using an electronic balance and its original dynamic elastic modulus was determined with a DT-20 dynamic elastic modulus tester. The specimen was placed into the test box, ensuring a 20 mm distance between neighboring specimens, and a minimum distance of 20 mm was maintained between the specimen and the side walls of the test box. The prepared 5% Na_2SO_4 solution was injected into the instrument's liquid tank. This concentration references field measurements from coastal saline soils and typical sulfate erosion regions in China (e.g., areas surrounding salt lakes in Northwest China), where sulfate content typically ranges from 3% to 6%. A 5% concentration simulates actual service environments with moderate to severe erosion levels and is a commonly used accelerated erosion concentration in relevant research. The Na_2SO_4 solution was prepared from anhydrous sodium sulfate produced by Tianjin Dengfeng Chemical Reagent Factory. The test process for the concrete simulation of a sulfate erosion dry–wet cycle is shown in

Figure 4. The pH value of the Na_2SO_4 solution was measured in the upper and lower water tanks every 15 dry–wet cycles to ensure that the pH value was between 6 and 8. For the solution renewal frequency, a fixed cycle of renewal every 7 days was adopted. During each renewal, the old solution in the immersion container was completely replaced with fresh 5% Na_2SO_4 solution to maintain stable erosion ion concentration and prevent a decrease in erosion rate due to ion depletion. Otherwise, the solution was prepared anew [20]. At the end of 0, 30, 60, and 90 wet–dry cycles (with volume doping), the mass of the test specimen was measured, the dynamic elastic modulus was determined using a DT-20 dynamic elastic modulus tester, and the cubic compressive strength was measured using a DYE-2000S microcomputer servo pressure testing machine. Specimens from 120 tests were preserved for SEM microanalysis using an electron microscope.



Figure 3. Simulated sulfate erosion—dry and wet cycling tester.

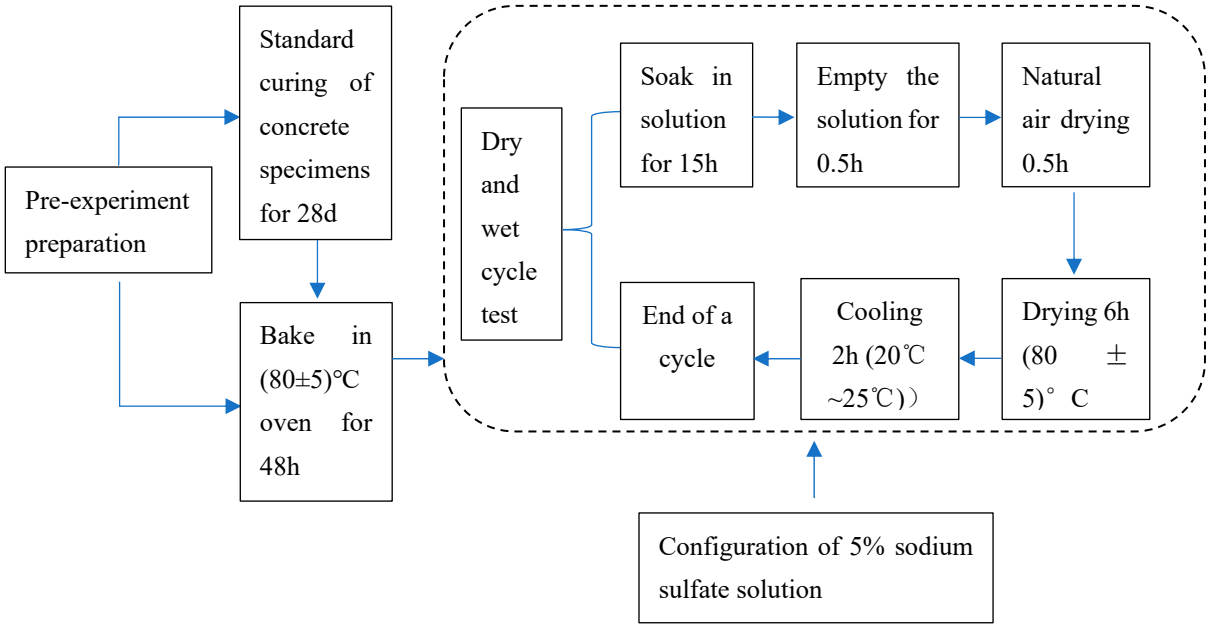

Figure 4. Simulated sulfate erosion of concrete—dry and wet cycling test procedure.

3.1. Epimorphology and Microanalysis

At the end of each wet–dry cycle, the apparent morphology of the specimens in each group was observed, photographed, and recorded. A comparison was made between different types of fibers, the number of wet–dry cycles, and the variations in specimens with different fiber dosages. SEM scanning was performed on the specimens after 120 cycles. The 120 wet–dry cycles established in this study are based on preliminary experimental results and literature reports. This cycle count induces noticeable erosion damage in concrete and correlates well with the natural erosion effects observed in actual engineering projects over 5 to 10 years. It provides reliable accelerated test data for subsequent service life prediction. The electron microscope allowed the visualization of the changes in the internal cracks and voids in the recycled concrete due to the wet–dry cycles, as well as the effect of the fibers on the material. An intuitive explanation of the decrease in macroscopic indices caused by sulfate wet–dry cycling on recycled concrete is provided as follows.

3.2. Rate of Quality Loss

An electronic balance was used to measure the mass of each group of specimens after different numbers of wet–dry cycles, with an accuracy of 0.001 kg. The average mass of each group was used as the determined value. The formula for the mass loss rate is as follows:

$$W_i = \frac{M_o - M_i}{M_o} \times 100\% \quad (1)$$

where W_i is the mass loss rate of the specimen after i wet–dry cycles, M_o is the initial mass of the specimen before the wet–dry cycles (kg), and M_i is the mass of the specimen after i wet–dry cycles (kg).

3.3. Relative Dynamic Modulus of Elasticity

The transverse fundamental frequency and dynamic elastic modulus of the specimen were measured using the DT-20 dynamic elastic modulus tester, and the test apparatus is shown in Figure 5. The relative dynamic elastic modulus was calculated using the following formula:

$$E_i = \frac{f_i^2}{f_o^2} \times 100\% \quad (2)$$

where E_i is the relative dynamic elastic modulus of the specimen after i dry and wet cycles (dimensionless); f_o is the initial self-oscillation frequency of the specimen before the dry and wet cycles (Hz); and f_i is the self-oscillation frequency of the specimen after i dry and wet cycles (Hz).

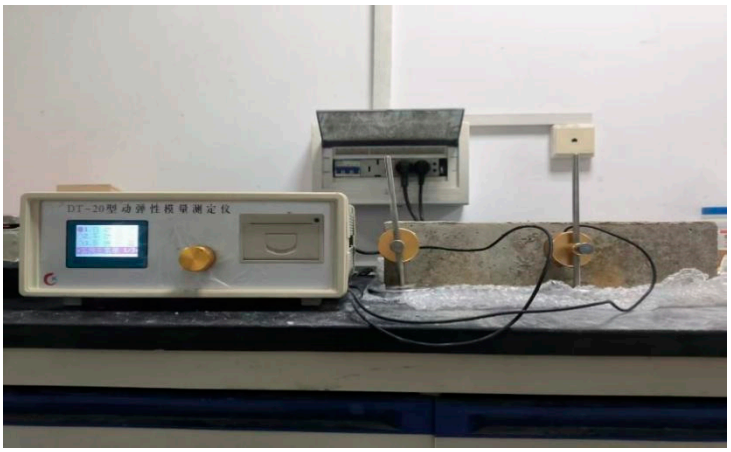

Figure 5. DT-20 dynamic elastic modulus tester.

3.4. Compressive Strength Durability Coefficient

The cube compressive strength of the specimen was determined using the DYE-2000S microcomputer servo pressure testing machine, as shown in Figure 6. The formula for calculating the compressive strength corrosion resistance coefficient is as follows:

$$S_c = \frac{c_i}{c} \tag{3}$$

where S_c is the compressive strength corrosion resistance coefficient, c_i is the compressive strength of the specimen after i cycles of wet and dry conditions (MPa), and c is the compressive strength of a group of contrasting specimens of the same age subjected to sulfate corrosion under standard maintenance conditions (MPa).

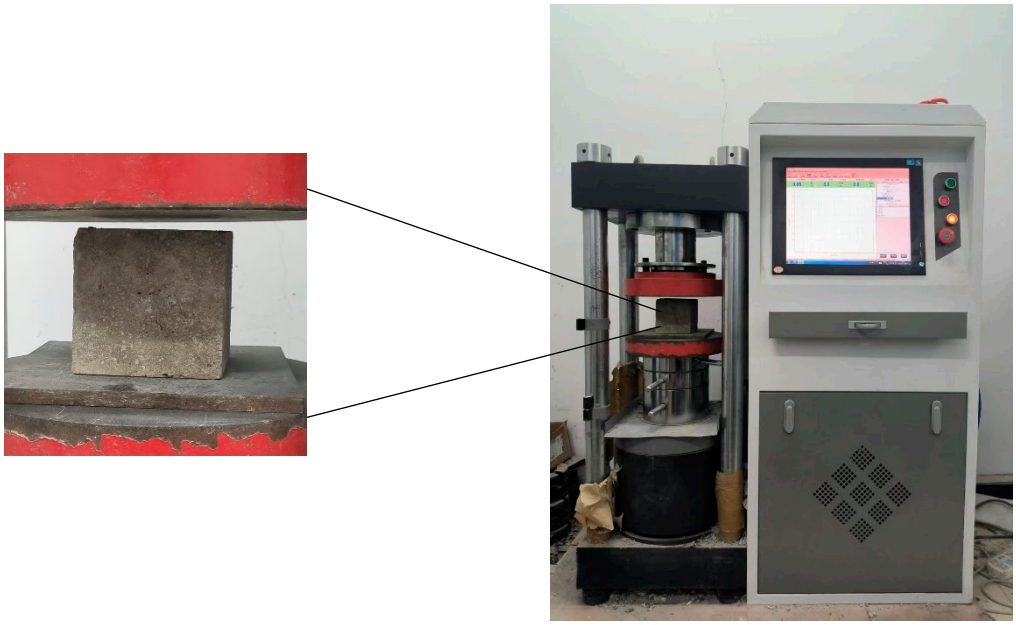

Figure 6. DYE-2000S microcomputer servo pressure testing machine.

3.5. Split Tensile Strength Corrosion Resistance Factor

The formula for calculating the splitting tensile strength corrosion resistance coefficient is as follows:

$$S_t = \frac{t_i}{t} \tag{4}$$

where S_t is the split tensile strength corrosion resistance coefficient; t_i is the split tensile strength (MPa) of the specimen after i cycles of wet and dry conditions; and t is the split tensile strength (MPa) of a set of contrasting specimens of the same age as the specimen, subjected to sulfate corrosion under standardized maintenance conditions.

4. Results and Discussion

4.1. Epimorphology and Microanalysis

4.1.1. Apparent Morphology

After the specimens had completed the standard curing process, they were removed from the curing room, and the surface of each group of specimens was observed. The C, RAC, and BFRAC specimens maintained their original appearance without significant changes, demonstrating good stability and durability. However, the SFRAC specimen developed yellow-brown rust stains. The reason for this phenomenon is that the relative humidity in the standard curing room is 95%, and this high humidity environment leads to a significant accumulation of water vapor, forming a thin film of water on the surface of the

specimen. For the SFRAC specimens, this water film acted as the medium for an oxidation reaction between the oxygen in the air and the steel fibers. Over time, the steel fibers gradually rusted on the surface of the specimen, leading to the formation of yellow-brown rust stains.

Figure 7 presents a comparison of the specimens with 1.5% steel fiber and bamboo fiber after different wet and dry cycles. Except for the increased corrosion of the SFRAC specimens after 30 wet–dry cycles, the surfaces of all other specimen groups showed minimal change, with no mortar shedding or corner flaking. After 60 wet–dry cycles, the SFRAC experienced increased rusting. Upon observing the surface of the SFRAC, it was noted that the steel fibers on the exterior had rusted and penetrated inward. In all specimens, the surface mortar exhibited white salt efflorescence. This occurs because when the specimen is immersed in a Na_2SO_4 solution, the SO_4^{2-} ions penetrate into the surface layer of the specimen through microcracks via capillary action, with the solution temperature ranging from 20 °C to 25 °C. During the early stage of the drying phase in the wet–dry cycle, as the temperature rises, the solubility of alkaline materials in the specimen increases. In the later stage of drying, with the continuous evaporation of liquid, salts form within the specimen and gradually precipitate to the surface, resulting in the formation of white salt efflorescence. This salt frost phenomenon is more pronounced in SFRAC due to the corrosion of the steel fibers on the surface.

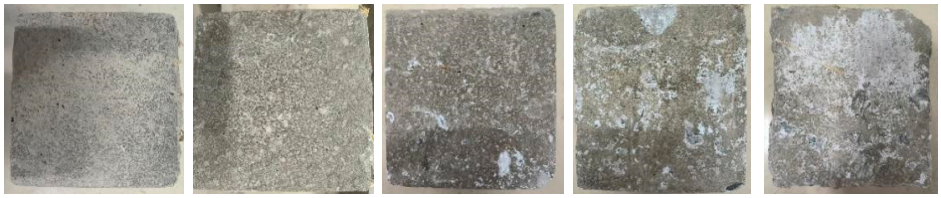

0 30 60 90 120

(**a**) Apparent morphology of BFRAC after various wet and dry cycles.



0 30 60 90 120

(**b**) Apparent morphology of SFRAC after various wet and dry cycles.

Figure 7. Apparent morphology of fiber-reinforced concrete after various wet and dry cycles.

When the number of wet–dry cycles reaches 90, the white frost crystallization on the surface of each group of specimens expands, and all of them exhibit slight cracks and minor mortar separation due to the "skinning" phenomenon. This is due to the expansion pressures generated by the reaction of sulfate with cement, producing ettringite and gypsum, as well as the crystallization of salts in the cracks during the drying process of the specimen. These processes can widen the cracks, initially formed by capillary action, into cracks visible to the naked eye. Simultaneously, the surface of the specimen is attacked by sulfate and undergoes chemical decomposition [21], leading to a looser structure and increased internal cracking. As a result, the specimen's surface becomes "skinned" under repeated wet and dry cycles. SFRAC corrosion becomes more severe, with the surface developing a reddish-brown layer of Fe_2O_3. The corrosion of the fibers penetrates the specimen, and the extent of corrosion becomes visible to the naked eye. When the steel fibers protruding from the specimen matrix are gently touched, they immediately fracture. When the number of wet and dry cycles reaches 120, the cracks in each group

of specimens expand, forming a network of cracks. The "skinning" phenomenon on the surface intensifies, and the shedding of mortar leads to an increase in the number of holes on the specimen's surface. At the same time, the previously "skinned" mortar on the specimen's surface gradually detaches due to the scouring effect of the sulfate solution and the repeated expansion stresses [22]. This study did not conduct sulfate permeability profiling tests, XRD/TG-DSC phase analysis, or EDS elemental mapping. Therefore, it is not possible to directly quantify the distribution and content of erosion products. The interpretation of "product accumulation/absorption" remains based on indirect inferences from macroscopic phenomena.

4.1.2. Micro-Analysis

SEM analysis is a crucial technical tool for optimizing material design, enhancing performance, and promoting the efficient use of construction waste. It visually presents the microscopic morphology, defects, and interfacial properties of recycled concrete, while correlating macroscopic performance with microscopic mechanisms. The results provide theoretical support for engineering applications and contribute to the development of green concrete technology. To better understand the internal erosion mechanism of concrete specimens subjected to sulfate erosion dry–wet cycles, surface and internal samples from C and 1.5% BFRAC specimens tested for 120 cycles were taken to characterize the microstructure of the corrosion products. The composition of the erosion products was analyzed using scanning electron microscopy (SEM) for microscopic evaluation [23], as shown in Figure 8.

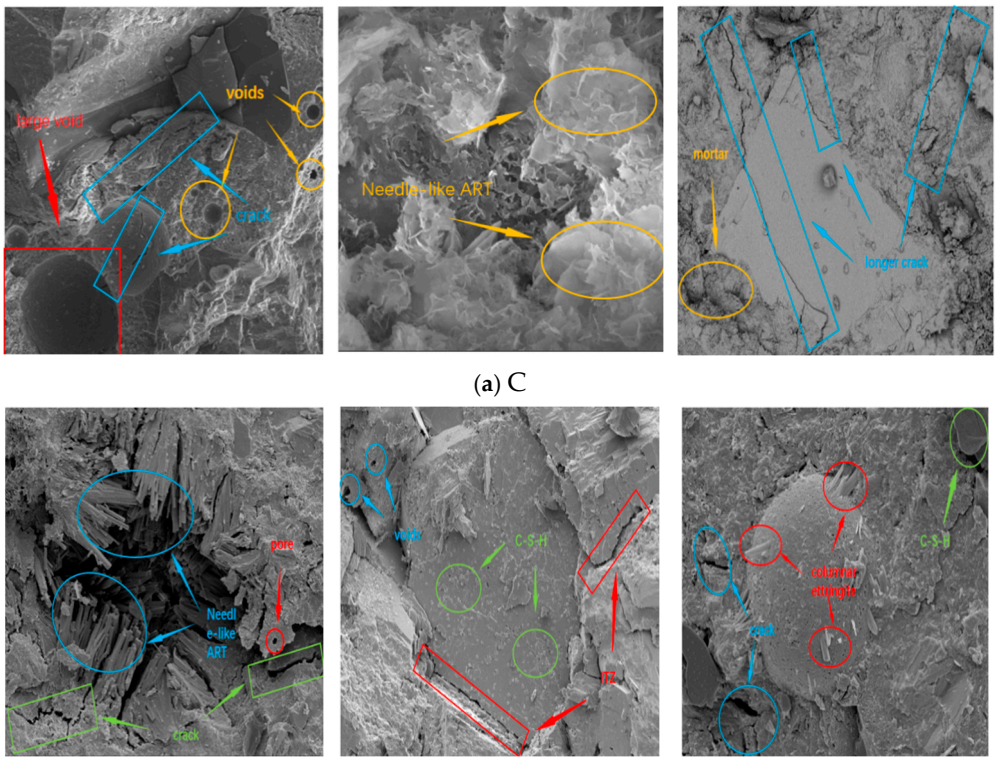

Figure 8. Internal microstructural morphology of specimens subjected to 120 sulfate attack cycles.

As shown in Figure 8a, in the absence of recycled aggregate (RAC), the microscopic image reveals large pores and cracks caused by insufficient bonding of the hydration products. Additionally, there is a distribution of granular bumps, leading to uneven hydration product formation. Locally, a small amount of gelling material is present, resulting in the formation of ettringites [24]. As shown in Figure 8b, when bamboo fiber (BF) was added at 1.5% and

recycled coarse aggregate (RAC) at 20%, cracks appeared at the interfacial transition zone (ITZ) and gradually diminished in size. Similarly, the holes also became smaller, indicating that the ettringites produced by RAC partially filled the larger pores and holes. The erosion reaction increases the amount of ettringites, and the ettringites generated within the matrix appear at pore defects. A large number of ettringite crystals accumulate in an intact state, completely wrapping the aggregate and forming a continuous structure, which helps to fill the pore space to some extent. Additionally, the intrusion of SO_4^{2-} accelerates the formation of calcium sulfoaluminate. Due to the weaker cohesion of the old mortar, it is the first to break its bond among the recycled aggregates. A large number of fibrous gels and gypsum crystals are closely connected and staggered. At this stage, the intact chalcocite is no longer visible, indicating that the erosion reaction has progressed more thoroughly. The C-H-S gel particles are more fully developed, with the gelled particles stacked on top of each other [25] and uniformly distributed on the surface of the unhydrated particles, forming a dense microscopic structure. SEM observations revealed that the pure thermal effect group exhibited only the dehydration of the matrix hydration products, with no sulfate-induced products such as calcite; in contrast, the sulfate erosion group showed distinct formation of erosion products, further validating the separation of damage effects.

4.2. Rate of Mass Loss

The damage to concrete specimens exposed to wet and dry cycles of sulfate erosion may not be fully evident in their external morphology. However, by analyzing changes in the specimens' quality, their sulfate resistance and durability can be better understood. According to the test procedure shown in Figure 4, specimens are weighed after every 15 wet–dry cycles. The change in the quality of each group of specimens is presented in Table 3 below.

Table 3. Mass of each specimen group after different numbers of wet–dry cycles (kg).

Specimen Number	Number of Wet and Dry Cycles (Times)								
	0	**15**	**30**	**45**	**60**	**75**	**90**	**105**	**120**
C	9.427	9.437	9.439	9.440	9.443	9.438	9.435	9.432	9.411
RAC	9.487	9.499	9.504	9.513	9.509	9.503	9.496	9.484	9.462
1%SFRAC	9.554	9.561	9.565	9.574	9.571	9.565	9.558	9.544	9.521
1.5%SFRAC	9.793	9.807	9.808	9.808	9.810	9.806	9.800	9.796	9.773
2%SFRAC	9.970	9.978	9.990	9.994	9.990	9.986	9.980	9.957	9.941
1%BFRAC	9.432	9.437	9.447	9.450	9.453	9.449	9.440	9.426	9.411
1.5%BFRAC	9.540	9.551	9.553	9.554	9.557	9.555	9.550	9.546	9.524
2%BFRAC	9.539	9.549	9.556	9.559	9.553	9.552	9.549	9.548	9.528

Using the data in Table 3 and the mass loss rate formula from Section 3.2, the mass loss rate for each group of specimens was calculated, as shown in Table 4 below.

Table 4. Mass loss rate for each specimen group after different numbers of wet–dry cycles (%).

Specimen Number	Number of Wet and Dry Cycles (Times)								
	0	**15**	**30**	**45**	**60**	**75**	**90**	**105**	**120**
C	0	−0.08	−0.13	−0.14	−0.17	−0.12	−0.08	−0.05	0.17
RAC	0	−0.13	−0.18	−0.27	−0.23	−0.17	−0.09	0.03	0.26
1%SFRAC	0	−0.10	−0.11	−0.21	−0.18	−0.11	−0.04	0.10	0.35
1.5%SFRAC	0	−0.14	−0.15	−0.15	−0.17	−0.13	−0.07	−0.03	0.20
2%SFRAC	0	−0.15	−0.20	−0.24	−0.20	−0.16	−0.10	0.13	0.29
1%BFRAC	0	−0.11	−0.16	−0.19	−0.22	−0.18	−0.09	0.06	0.22
1.5%BFRAC	0	−0.12	−0.14	−0.15	−0.18	−0.16	−0.11	−0.06	0.17
2%BFRAC	0	−0.14	−0.18	−0.21	−0.15	−0.14	−0.11	−0.09	0.12

The mass loss rate for each specimen group was calculated, and their variations are shown in Figure 9.

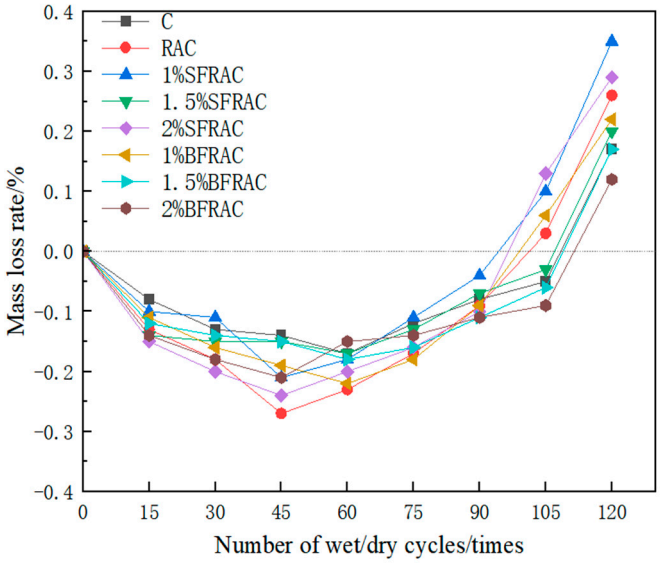

Figure 9. Mass loss rate of each specimen group under different wet–dry cycle conditions.

As shown in Figure 9, the mass of each specimen group initially increases and then decreases after undergoing sulfate erosion through wet–dry cycles. This behavior can be attributed to the inherent pores and cracks in the concrete material. During the initial stage of the test, the sulfate solution penetrates the specimen through capillary action, where it chemically reacts with the cement and remains in the specimen. In the later stages, sulfate erosion intensifies, causing the dissolution and precipitation of the collodion material, which leads to a decrease in the specimen's mass [26]. The mass reaches its peak after 45 to 60 cycles. After 105 wet–dry cycles, the specimen's mass essentially returns to its original value. The specific observations are as follows:

During the 0 to 15 wet–dry cycles, in the soaking stage, Na_2SO_4 solution enters the specimen through its cracks and pores due to capillary action. In the drying stage, the water evaporates, and the Na_2SO_4 solution inside the specimen becomes concentrated and crystallizes, resulting in an increase in the specimen's mass. When the number of wet–dry cycles ranges from 15 to 60, the pressure generated by the crystallization of Na_2SO_4 inside the specimen enlarges its cracks and pores, allowing more solution to penetrate during the immersion stage. Additionally, the sulfate solution continues to crystallize and precipitate, causing white frost to appear on the specimen's surface. At the same time, the Na_2SO_4 solution reacts with the cement, with sulfate reacting with aluminate in the hydration products to form ettringite, and sulfate reacting with calcium hydroxide to form gypsum. The expansion pressure caused by the formation of these solids further enlarges the cracks and pores in the specimens. Among them, RAC, 1%SFRAC, 2%SFRAC, and 2%BFRAC reach their maximum mass after 45 wet–dry cycles, with mass loss rates of −0.27%, −0.21%, −0.24%, and −0.21%, respectively. In contrast, C, 1.5%SFRAC, 1%BFRAC, and 1.5%BFRAC reach their maximum mass only after 60 wet–dry cycles. The rate of change in the mass loss of RAC is higher than that of C. This is because, during the pre-dry and wet cycles, the recycled aggregate is produced by crushing old concrete, resulting in more microscopic cracks compared to natural aggregate. As a result, water absorption is higher, allowing more Na_2SO_4 solution to penetrate the specimen, which makes the mass change more noticeable.

When the number of wet and dry cycles ranges from 60 to 105, the mass of each specimen decreases, but all remain greater than their original mass. This is because,

under continuous erosion by sulfate, the cementitious material in the cement is gradually destroyed and precipitated, reducing the mass. However, gypsum and calcium aluminate remain inside the specimen, preventing the mass from falling below its original value. The sulfate solution initially erodes the surface layer of the specimen. During the drying and evaporation process, the high concentration of sulfate solution accelerates the destruction of the cementitious structure on the surface, leading to a "skinning" phenomenon. Even a small amount of mortar loss due to this "skinning" can reduce the specimen's mass. When subjected to 105 to 120 wet and dry cycles, the quality of each group of specimens decreased to its lowest point, falling below the original quality. This deterioration is attributed to the shedding of the 'skinned' mortar from the specimen's surface after the application of Na_2SO_4 solution. Additionally, the expansion stress induced by gypsum and caliche cause the corners of the specimens to break, leading to a dramatic decrease in their quality.

4.3. Relative Dynamic Modulus of Elasticity

In sulfate-containing environments, concrete materials undergo significant erosive effects. Sulfate ions gradually penetrate the concrete and chemically react with the hydration products, forming bulkier crystalline substances. The accumulation of these crystalline substances within the concrete can cause micro-cracks and pores due to expansion pressure, which, in turn, compromises its original structural integrity. This series of chemical and physical processes directly results in a significant decrease in the concrete's modulus of elasticity, weakening its ability to resist deformation and impairing its overall mechanical properties".

To effectively assess the durability of concrete in harsh environments, the dynamic elastic modulus of the specimen is measured. By exciting the specimens and monitoring their vibration response, the dynamic elastic modulus can be accurately calculated, as it is sensitive to changes in the internal structure of the concrete. Based on long-term monitoring data and the trend of the dynamic elastic modulus, the remaining lifespan of concrete specimens can be scientifically predicted. This provides a crucial foundation for structural maintenance and reinforcement, while preventing the potential specimen damage associated with traditional testing methods.

According to the test procedure outlined in Figure 4, the specimens were removed every 15 wet and dry cycles. The transverse fundamental frequency and dynamic elastic modulus of each specimen were measured using the DT-20 dynamic elastic modulus tester. The relative dynamic elastic modulus for each group of specimens, corresponding to different numbers of wet and dry cycles, was calculated based on the formula in Section 3.3, as shown in Table 5.

Table 5. Relative dynamic elastic modulus of each group of specimens under different numbers of wet and dry cycles (%).

Specimen Number	Number of Wet and Dry Cycles (Times)								
	0	**15**	**30**	**45**	**60**	**75**	**90**	**105**	**120**
C	100	100.53	101.31	101.95	102.21	101.77	99.47	95.16	90.39
RAC	100	101.98	102.91	103.86	102.03	101.52	97.11	92.56	85.42
1%SFRAC	100	100.68	101.39	103.03	102.86	100.63	96.73	90.33	86.45
1.5%SFRAC	100	102.24	102.57	102.15	102.57	101.87	98.79	94.40	89.40
2%SFRAC	100	101.20	103.28	103.40	103.18	101.36	97.68	90.72	86.43
1%BFRAC	100	100.17	102.33	102.70	103.50	101.66	97.79	92.32	87.74
1.5%BFRAC	100	101.76	102.01	102.05	102.86	102.10	98.98	95.32	90.39
2%BFRAC	100	102.03	102.91	103.16	102.31	101.07	99.23	95.87	88.64

Based on the data in Table 5, the relative dynamic modulus of elasticity for each group of specimens, corresponding to different numbers of wet and dry cycles, was plotted, as shown in Figure 10.

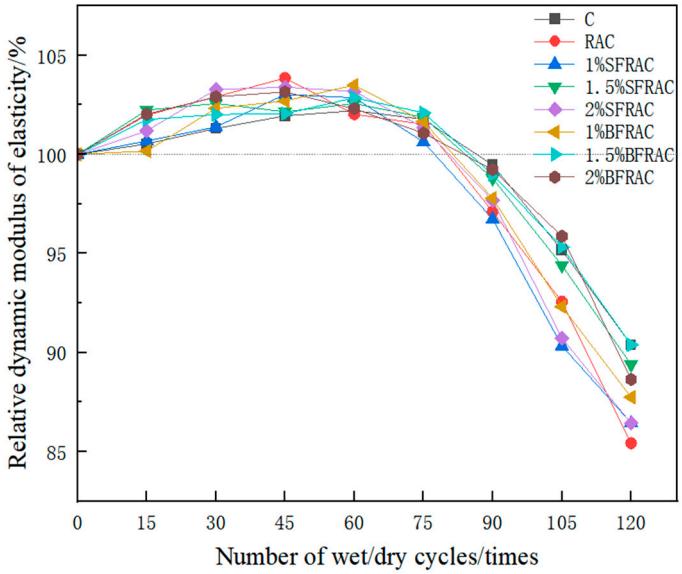

Figure 10. Relative dynamic elastic modulus of each group of specimens under different wet and dry cycling conditions.

It is evident from Figure 10 that, under the specific environmental condition of sulfate wet and dry cycling, the relative dynamic elastic modulus of the specimens follows a trend closely resembling the rate of mass change, both first increasing and then decreasing. In the initial stage of the dry–wet cycle, the relative dynamic elastic modulus of the specimens exhibits a significant upward trend. This phenomenon can primarily be attributed to a series of complex chemical reactions occurring within the concrete due to the alternation between wet and dry conditions. Particularly critical is the generation of C-S-H (calcium silicate hydrate). C-S-H is a key contributor to the strength of concrete, gradually filling the pores and densifying the internal structure. This densification process effectively enhances the modulus of elasticity of the concrete, resulting in an increase in the relative dynamic modulus of elasticity. The relative dynamic elastic modulus of RAC and C after 15 wet–dry cycles is 102.91% and 101.31%, respectively, with RAC showing a higher value than C. This difference is due to the greater number of cracks in RAC, which allow more sulfate solution to penetrate during the wet–dry cycling. This leads to the formation of calcium aluminate and gypsum crystals, which densify the specimen in the early stages, resulting in a higher relative dynamic elastic modulus. This behavior is consistent with the findings of J. Haufe et al. [27].

However, as the wet–dry cycles progressed, the relative dynamic modulus of elasticity of the specimens gradually decreased. This decline was attributed to the expansion stresses caused by the crystallization of calcite and gypsum [28], which expanded the cracks within the specimens and compromised the structural integrity of the concrete. Under the influence of wet–dry cycles, sulfate that penetrates the concrete will undergo a process of crystallization, dissolution, and recrystallization. When the concentration of sulfate exceeds its solubility, it will crystallize and precipitate, generating crystallization pressure, which exerts a destructive effect on the concrete. Especially under wet–dry cycling conditions, the evaporation of water from the concrete surface leads to an increase in sulfate concentration and crystallization pressure, making the destructive effect on the concrete more pronounced [29]. Additionally, during the drying process, the specimen is subjected to thermal pressure at a high temperature

of 80 °C. Therefore, under the combined effects of expansion stress, salt crystallization stress, and temperature stress, the specimens began to experience internal damage, resulting in a decrease in the relative dynamic elastic modulus. When the number of wet–dry cycles reached 120, the relative dynamic elastic modulus of the specimens with 1%, 1.5%, and 2% steel fiber doping were 86.45%, 89.4%, and 86.43%, respectively. The relative dynamic elastic modulus of the specimens with 1%, 1.5%, and 2% bamboo fiber doping were 87.74%, 90.39%, and 88.64%, respectively. It can be observed that at the end of the wet–dry cycles, the relative dynamic elastic modulus of bamboo fiber concrete was slightly higher than that of steel fiber concrete. Additionally, the relative dynamic elastic modulus of all specimen groups remained above 60%. This indicates that none of the specimens failed or sustained damage after 120 sulfate wet–dry cycles and can be used normally.

4.4. Compressive Strength Corrosion Resistance Factor

Generally, a concrete specimen with higher compressive strength is less susceptible to structural damage from external pressures during prolonged use [30,31]. However, sulfate erosion can cause the formation of expansion products within the concrete, such as ettringite, which may deteriorate the concrete's microstructure and result in a reduction in strength. By measuring the changes in compressive strength of concrete specimens after sulfate dry and wet cycling tests, the degradation of concrete's properties in an erosive environment can be assessed, thus allowing for the evaluation of its durability. Comparing the variations in compressive strength of the specimens across different cycles reveals the mechanisms and processes involved in sulfate erosion.

Three sets of cubic specimens were taken for compressive testing after every 15 wet and dry cycles. The results of these tests are presented in Table 6 below.

Table 6. Cubic compressive strength of each group of specimens under different numbers of dry and wet cycles (MPa).

Specimen Number	Cubic Compressive Strength (MPa)								
	0	**15**	**30**	**45**	**60**	**75**	**90**	**105**	**120**
C	51.33	52.88	53.45	53.84	54.11	53.73	52.52	50.28	47.76
RAC	46.43	48.55	49.13	49.63	48.88	48.54	46.45	44.30	40.90
1%SFRAC	49.43	51.02	51.52	52.40	52.42	50.18	48.23	42.98	41.05
1.5%SFRAC	46.83	49.09	49.38	50.26	51.55	49.11	45.62	41.54	37.15
2%SFRAC	45.00	46.71	47.82	49.89	47.92	45.97	42.26	40.09	35.11
1%BFRAC	48.13	49.42	50.64	50.88	52.38	50.34	48.45	45.79	42.13
1.5%BFRAC	46.57	48.60	48.86	49.92	51.42	48.94	47.48	44.75	39.80
2%BFRAC	43.47	45.49	47.04	48.00	47.50	46.28	43.46	40.96	35.33

Based on the data in Table 6 and the compressive strength corrosion resistance coefficient formula in Section 3.4, the corrosion resistance coefficient of compressive strength for each group of specimens is calculated and presented in Table 7.

Table 6 shows that the compressive strength of 1% SFRAC is slightly higher than that of RAC when the number of wet and dry cycles reaches 120, indicating that the addition of an appropriate amount of steel fibers can still improve the compressive strength of the specimens under wet and dry cycles. However, Table 7 shows that the corrosion resistance coefficient of the cubic compressive strength of 1% SFRAC is lower than that of RAC, which suggests that, as the number of wet and dry cycles increases, the compressive strength enhancement from the addition of steel fibers to the specimens gradually diminishes. At 120 wet and dry cycles, the compressive strength and corrosion resistance coefficients of BFRAC are higher than those of SFRAC with the same fiber dosage. This may be

because in the later stages of wet and dry cycles, the steel fibers rust and swell, generating more expansion stress, which causes more cracks inside the specimen, thereby reducing its compressive strength. Bamboo fibers, however, do not corrode, so under the same fiber dosage, BFRAC produces relatively fewer cracks than SFRAC, resulting in a higher compressive strength and corrosion resistance coefficient.

Table 7. Corrosion resistance coefficients of compressive strength for each group of specimens under different numbers of wet and dry cycles (%).

Specimen Number	Cubic Compressive Strength Corrosion Resistance Factor (%)								
	0	**15**	**30**	**45**	**60**	**75**	**90**	**105**	**120**
C	100	103.02	104.13	104.89	105.42	104.68	102.32	97.95	93.05
RAC	100	104.57	105.82	106.89	105.28	104.54	100.04	95.41	88.09
1%SFRAC	100	103.22	104.23	106.01	106.05	101.52	97.57	86.95	83.05
1.5%SFRAC	100	104.83	105.45	107.32	110.08	104.87	97.42	88.70	79.33
2%SFRAC	100	103.80	106.27	110.87	106.49	102.16	93.91	89.09	78.02
1%BFRAC	100	102.68	105.22	105.71	108.83	104.59	100.66	95.14	87.53
1.5%BFRAC	100	104.36	104.92	107.19	110.41	105.09	101.95	96.09	85.46
2%BFRAC	100	104.65	108.21	110.41	109.28	106.46	99.98	94.23	81.27

Based on the data in Table 7, the corrosion resistance coefficients of the cubic compressive strength of each group of specimens were drawn as shown in Figure 11.

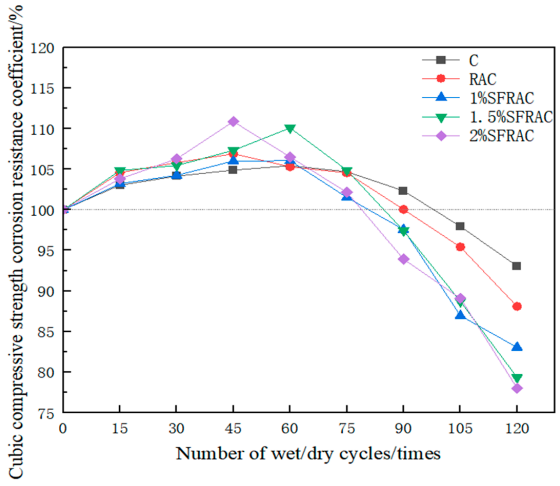

(**a**) Corrosion resistance coefficient of compressive strength of steel fiber specimens under different wet and dry cycles

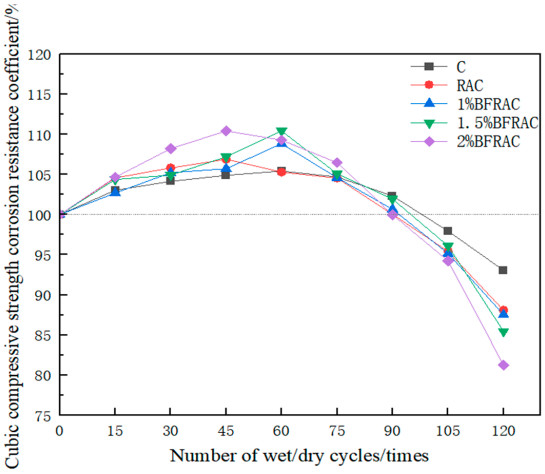

(**b**) Corrosion resistance coefficient of compressive strength of bamboo fiber specimens under different wet and dry cycles

Figure 11. Corrosion resistance coefficient of cubic compressive strength under different wet and dry cycles.

The compressive strength of each group of specimens initially increased with the number of wet and dry cycles, followed by a decline. Between 45 and 60 cycles, the compressive strength and corrosion resistance coefficient reached their maximum values. After that, both began to decrease, and by around 90 cycles, they had returned to their original state. This behavior occurs because concrete undergoes wetting and drying processes during the wet and dry cycles. When the concrete is wet, the sulfate solution penetrates its pores. During the drying phase, the water evaporates, potentially causing the sulfate to crystallize or allowing the accumulation of reaction products in the pores. This results in the filling of the pores, an increase in densification, and ultimately a rise in strength. Additionally, all specimens were mixed with fly ash, and the high temperatures during the drying phase of the sulfate wet–dry cycle served as a catalyst to promote secondary hydration, generating additional C-S-H gels that further densified the structure.

The figure shows that the compressive strength of each group of specimens reaches its maximum between the 45th and 60th cycle, after which it decreases. This is due to the generation of calcium aluminate and gypsum, which are accompanied by volumetric expansion. The repeated wet–dry cycles result in the continuous accumulation of expansion products in the pore space and interfacial transition zone (ITZ), creating internal tensile stresses that trigger the formation and growth of microcracks. Additionally, the repeated migration of water during the cycling process exacerbates physical effects, such as temperature and shrinkage stresses, and accelerates structural deterioration in combination with chemical erosion.

Comparing Figure 11a,b, when the number of wet and dry cycles has not reached 90, the compressive strength and corrosion resistance coefficient of SFRAC are lower than their initial values, while BFRAC remains at or above the initial value. However, when the number of wet and dry cycles reaches 120, the compressive strength and corrosion resistance coefficient of all steel fiber specimens fall below those of RAC. As the amount of steel fiber doping increases, the compressive strength and corrosion resistance coefficients of the specimens decrease progressively. At 1% bamboo fiber doping, the compressive strength and corrosion resistance coefficient of the specimens approach those of RAC, but as the bamboo fiber doping level increases further, both the compressive strength and corrosion resistance coefficient continue to decrease. The compressive strength and corrosion resistance coefficient of the specimens decreased by 5.72%, 9.94%, and 11.43% at steel fiber dosages of 1%, 1.5%, and 2%, respectively. For bamboo fiber dosages of 1%, 1.5%, and 2%, the compressive strength and corrosion resistance decreased by 0.64%, 2.99%, and 7.74%, respectively.

4.5. Split Tensile Strength Corrosion Resistance Factor

The splitting tensile strength of concrete is a crucial indicator of its resistance to cracking. Under the combined effects of sulfate erosion and wet–dry cycles, the internal microstructure of the concrete undergoes changes, leading to a reduction in mechanical properties and a decrease in crack resistance. By conducting splitting tensile tests with varying numbers of wet and dry cycles, the changes in the cracking resistance of concrete at different stages of erosion can be observed, providing a foundation for evaluating the durability and service life of concrete.

Three sets of cubic specimens were removed after every 15 wet and dry cycles for splitting tensile testing. The results of the convergent tests are presented in Table 8 below.

Table 8. Cube splitting tensile strength (MPa).

Specimen Number	Cube Splitting Tensile Strength (MPa)								
	0	**15**	**30**	**45**	**60**	**75**	**90**	**105**	**120**
C	3.32	3.43	3.58	3.61	3.71	3.54	3.31	2.99	2.61
RAC	2.85	3.00	3.09	3.12	3.04	2.86	2.63	2.29	2.08
1%SFRAC	3.28	3.49	3.60	3.62	3.53	3.40	3.16	2.88	2.42
1.5%SFRAC	3.53	3.73	3.82	3.92	3.82	3.55	3.20	3.10	2.73
2%SFRAC	3.66	3.90	3.99	3.90	3.78	3.61	3.32	2.99	2.42
1%BFRAC	3.18	3.40	3.49	3.55	3.49	3.36	3.14	2.84	2.43
1.5%BFRAC	3.47	3.61	3.77	3.86	3.94	3.79	3.57	3.21	2.75
2%BFRAC	3.57	3.74	3.84	3.78	3.69	3.57	3.39	2.94	2.53

Based on the data in Table 8 and the formula for the split tensile strength corrosion resistance coefficient in Section 3.5, the corrosion resistance coefficients for the split tensile strength of each group of specimens were calculated, as shown in Table 9 below.

Table 9. Corrosion resistance coefficients for the split tensile strength of each group of specimens under different numbers of wet and dry cycles (%).

Specimen Number	Cube Split Tensile Strength Corrosion Resistance Factor (%)								
	0	**15**	**30**	**45**	**60**	**75**	**90**	**105**	**120**
C	100	103.35	107.88	108.61	111.87	106.56	99.56	90.19	78.64
RAC	100	105.09	108.45	109.45	106.68	100.49	92.19	80.33	72.96
1%SFRAC	100	106.52	109.89	110.45	107.56	103.81	96.42	87.68	74.23
1.5%SFRAC	100	105.65	108.24	110.98	108.31	100.68	90.56	87.74	77.38
2%SFRAC	100	106.68	108.89	106.56	103.28	98.69	90.68	81.56	66.27
1%BFRAC	100	106.87	109.77	111.54	109.76	105.73	98.75	89.42	76.45
1.5%BFRAC	100	104.16	108.56	111.27	113.45	109.28	102.75	92.65	79.17
2%BFRAC	100	104.88	107.63	105.78	103.28	100.03	94.84	82.38	70.75

Based on the data in Table 9, the corrosion resistance coefficients of the cube split tensile strength for each group of specimens were plotted, as shown in Figure 12.

As shown in Figure 12a, the split tensile strength corrosion resistance coefficients of all specimen groups initially increase and then decrease as the number of wet and dry cycles increases. However, the timing of when each group reaches its maximum value varies significantly. The tensile resistance of RAC peaks earlier than that of C. The tensile resistance of SFRAC reaches its peak earlier as the fiber content increases, while BFRAC reaches its peak at 1.5% fiber content. This is consistent with the findings of the study by Min Dai Dai [32], which shows a more significant enhancement effect of bamboo fiber on the splitting tensile strength of concrete specimens.

The reason the tensile and corrosion resistance coefficient of RAC reaches its maximum value before that of C is that the recycled aggregate in RAC contains more cracks, allowing more sulfate solution to intrude into the concrete pores by capillary action. This, in turn, chemically reacts with the cement hydration products to form compounds such as calcium alumina and gypsum. These products initially fill the pores and micro-cracks within the concrete, making the structure denser, thus increasing its tensile strength. The performance of SFRAC may be attributed to its higher steel fiber content. As more steel fibers are slightly oxidized in the early stage, the surface of the oxidized fibers undergoes slight corrosion. When this corrosion results in stress expansion that does not exceed the maximum pressure that the specimen can withstand, it makes the specimen denser. Consequently, the specimen's split tensile strength and corrosion resistance coefficient also increase. Bamboo fiber, however, does not rust, so its tensile strength and corrosion resistance coefficient take longer to reach their maximum values.

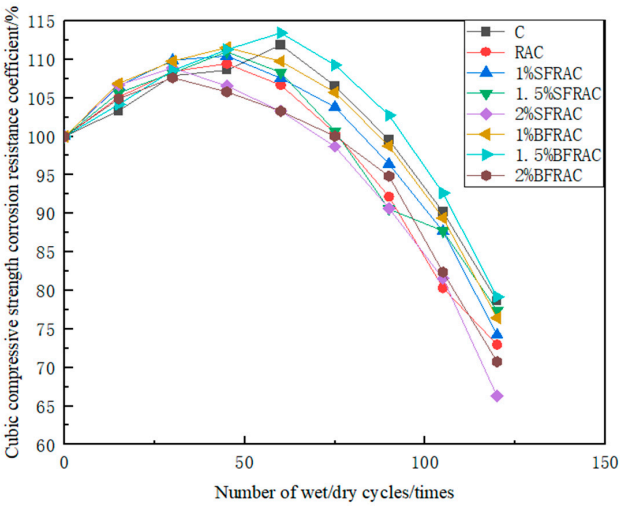

(**a**) Corrosion resistance coefficients of split tensile strength of each group of specimens under different wet and dry cycles

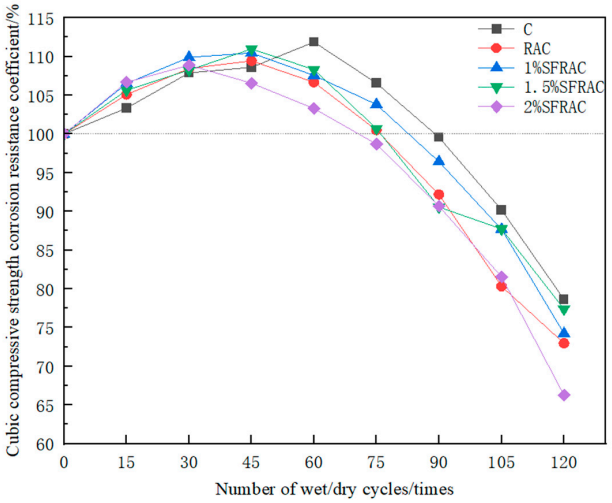

(**b**) Corrosion resistance coefficient of split tensile strength of steel fiber specimens under different wet and dry cycles

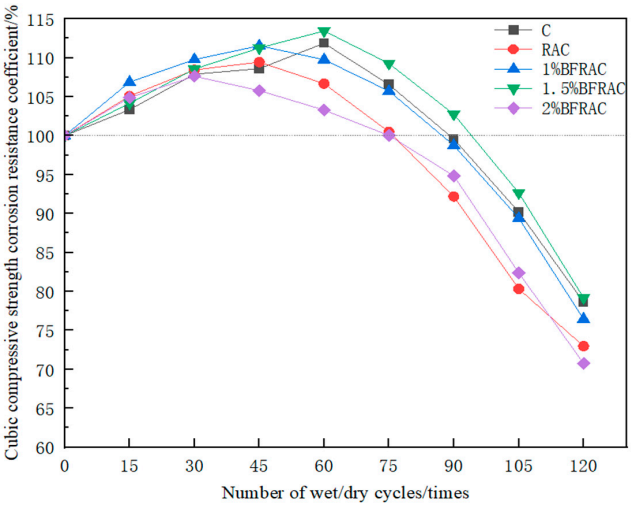

(**c**) Corrosion resistance coefficient of split tensile strength of bamboo fiber specimens under different wet and dry cycles

Figure 12. Corrosion resistance coefficients of cubic split tensile strength under different wet and dry cycles.

The tensile corrosion resistance coefficients of each group of specimens generally maintain their original values after 75 to 90 wet and dry cycles. However, these coefficients

decrease rapidly once the number of cycles exceeds 90, reaching their lowest point after 120 cycles.

Comparing Figure 12b,c, both SFRAC and BFRAC exhibited an initial increase followed by a decrease in the tensile strength corrosion resistance coefficient of the specimens as fiber doping increased after 120 wet and dry cycles. This is because when the fiber doping is below 1.5%, an increase in fiber content enhances the bridging effect within the specimen, thereby improving its tensile strength. However, when the fiber doping exceeds 1.5%, a higher fiber content results in an increased number of interfacial transition zones (ITZs) between the fibers and the cement, as well as between the fibers and the slurry. These ITZs become weakened due to sulfate attack, which creates a preferential path for crack propagation, thereby accelerating the loss of tensile strength. With the same fiber dosage, BFRAC exhibits higher tensile strength and corrosion resistance compared to SFRAC. This can be attributed to the fact that the strength of the interfacial transition zone (ITZ) in SFRAC relies on the bond between the mortar and the steel fibers. Once the steel fibers corrode, not only is the tensile strength of the fibers significantly reduced, but the corrosion also weakens the expansion pressure generated within the specimen. This leads to internal damage and the formation of cracks, significantly reducing both the tensile strength and corrosion resistance of the specimen. Consequently, the corrosion resistance coefficient and tensile strength of the specimen are greatly diminished. In contrast, the bamboo fibers are pre-soaked and saturated with water before preparing BFRAC. As a result, after the specimen is formed, the cement undergoes further hydration with the water inside the bamboo fibers, which leads to a stronger interfacial transition zone (ITZ). Additionally, bamboo fibers do not corrode, so there is no expansion pressure that could damage the interior of the specimen due to corrosion. The tensile strength and corrosion resistance of the specimens increase by 1.74%, 6.06%, and −9.17% at steel fiber dosages of 1%, 1.5%, and 2%, respectively. When bamboo fibers are incorporated at 1%, 1.5%, and 2%, the tensile strength and corrosion resistance of the specimens increase by 4.78%, 8.51%, and −3.03%, respectively.

5. Modeling Wet and Dry Cycle Injuries

5.1. Theoretical Foundations of the Weibull Distribution

The Weibull distribution is highly valuable as a continuous probability distribution, and is commonly used in reliability engineering. To predict the durability of concrete in sulfate dry and wet cyclic erosion environments, the two-parameter Weibull distribution model can be applied [32]. The model is based on the central assumption that the durability life, T of concrete follows a two-parameter Weibull distribution.

When using the two-parameter Weibull distribution for prediction, attention must be given to estimating two key parameters: the shape parameter and the scale parameter. The shape parameter determines the morphology of the distribution curve, reflecting the degree of variation in concrete durability life. The scale parameter, on the other hand, determines the scale of the distribution curve, representing the average or central tendency of concrete durability life. Accurate estimation of these two parameters is crucial for improving the accuracy and reliability of the prediction results.

By accurately estimating the shape and scale parameters, a reliable function that describes the durability life of concrete can be established. This function not only provides a method for quantitatively assessing the durability life of concrete in a specific environment but also offers a scientific basis for engineering design and maintenance decisions, which is crucial for ensuring the long-term safety and durability of concrete structures.

Distribution function F(t):

$$F(t) = 1 - \exp\left[-\left(\frac{t}{\theta}\right)^m\right] \tag{5}$$

Reliability function R(t):

$$R(t) = 1 - F(t) = \exp\left[-\left(\frac{t}{\theta}\right)^m\right] \tag{6}$$

where m is the shape parameter, m > 0; θ is the scale parameter, $\theta > 0$; and t is the time of the dry–wet cycle of sulfate, t > 0.

There is an inverse relationship between the reliability of concrete and its service life, meaning that the reliability of concrete structures decreases over time. Under normal conditions, due to material aging, the cumulative effect of loads, and other factors, the performance of concrete structures gradually weakens, thereby reducing their reliability. When exposed to severe environmental factors such as extreme weather or chemical attacks, the rate of this decline in reliability is further accelerated. Typically, $0 \leq R(t) \leq 1$. A threshold value is set such that when the reliability of the concrete decreases to 0 or below, it indicates that the concrete structure has reached its bearing capacity limit, meaning it has failed and can no longer safely perform its intended function. This threshold also corresponds to the number of dry and wet sulfate cycles experienced by the specimen at the point of failure and destruction, which represents the predicted service life.

5.2. Parameter Estimation of Relative Dynamic Modulus of Elasticity

The change in the relative dynamic elastic modulus evaluation parameter is used as the damage variable for concrete corrosion deterioration, i.e.,

$$D = \frac{1 - E_i}{0.4} \tag{7}$$

where D is the damage degree of the concrete specimen, $0 \leq D \leq 1$. When $D \geq 1$, this indicates that the regenerated concrete specimen has failed due to damage, while when D < 0, this indicates that the regenerated concrete specimen is in its normal service stage.

The parameter estimation of the Weibull distribution is typically performed using the least squares method. The distribution function and reliability function are formulated to model the durability degradation of concrete under the combined effects of "wet–dry cycling and sulfate erosion". Given the simplicity and practicality of the least squares method, as well as its high efficiency in calculating the parameters of linear functions, the process begins with a logarithmic transformation of the reliability function. Subsequently, the least squares method is employed to estimate the parameters of the transformed function. This method is selected not only for its ability to simplify the calculation process but also for its capacity to improve the accuracy of parameter estimation. Thus, taking the logarithm of the reliability function yields:

$$\ln[-\ln R(t)] = m \ln t - m \ln \theta \tag{8}$$

Such that $y = \ln[-\ln R(t)]$, $x = \ln t$ reduces to

$$y = ax + b \tag{9}$$

Such that $y = \ln[-\ln R(t)]$, $x = \ln t$ reduces to

The results of the two-parameter Weibull parameter calculations for each group of specimens are shown in Table 10.

Table 10. Weibull parameters.

Specimen Number	Shape Parameter/m	Scale Parameter/θ
C	5.372	185.684
RAC	6.983	166.015
1%SFRAC	9.854	148.185
1.5%SFRAC	8.788	164.238
2%SFRAC	9.037	158.430
1%BFRAC	6.160	183.556
1.5%BFRAC	5.225	203.774
2%BFRAC	6.457	177.651

5.3. Reliability Analysis and Life Prediction Based on Two-Parameter Weibull Distribution

After determining the shape parameter m and scale parameter θ in the table above, these parameters are substituted into the formula to derive the sulfate wet–dry cycling damage evolution equations for each group of specimens, as shown in Table 11 below.

$$D(t) = 1 - \exp\left[-\left(\frac{t}{185.684}\right)^{5.372}\right] \tag{10}$$

Table 11. Damage evolution equations.

Specimen Number	Damage Evolution Equation
C	$D(t) = 1 - \exp\left[-\left(\frac{t}{185.684}\right)^{5.372}\right]$
RAC	$D(t) = 1 - \exp\left[-\left(\frac{t}{166.015}\right)^{6.983}\right]$
1%SFRAC	$D(t) = 1 - \exp\left[-\left(\frac{t}{148.185}\right)^{9.854}\right]$
1.5%SFRAC	$D(t) = 1 - \exp\left[-\left(\frac{t}{164.238}\right)^{8.788}\right]$
2%SFRAC	$D(t) = 1 - \exp\left[-\left(\frac{t}{158.430}\right)^{9.037}\right]$
1%BFRAC	$D(t) = 1 - \exp\left[-\left(\frac{t}{183.556}\right)^{6.160}\right]$
1.5%BFRAC	$D(t) = 1 - \exp\left[-\left(\frac{t}{203.774}\right)^{5.225}\right]$
2%BFRAC	$D(t) = 1 - \exp\left[-\left(\frac{t}{177.651}\right)^{6.457}\right]$

The shape parameter m and scale parameter θ from Table 11 can be to obtain the predicted lifespan of each group of specimens under sulfate wet–dry cycling conditions. Additionally, the predicted number of cycles of resistance to sulfate wet–dry cycling for each group of specimens is calculated, as shown in Table 12 below.

Table 12. Predicted life of each group of specimens.

Specimen Number	Predicted Lifetime (Times)
C	262
RAC	216
1%SFRAC	180
1.5%SFRAC	202
2%SFRAC	194
1%BFRAC	244
1.5%BFRAC	290
2%BFRAC	237

Using Table 10, which presents the Weibull parameters for each group of specimens, the shape parameter m and scale parameter θ are substituted into Equation 5.1 to generate the reliability function $R(t)$ curve, as shown in Figure 13.

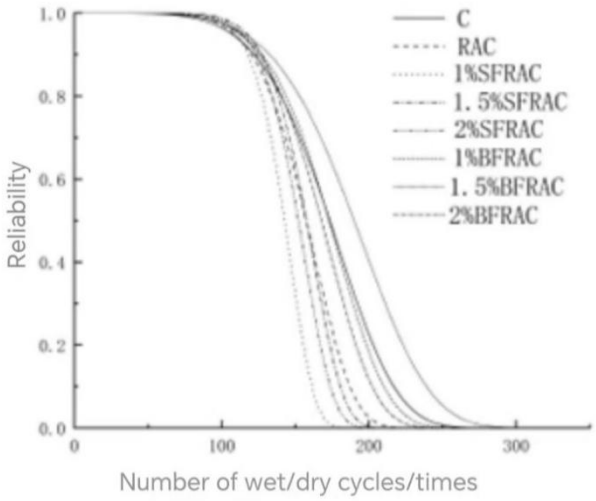

Figure 13. Reliability life prediction curves for each group of specimens.

As shown in Figure 13, BFRAC exhibits greater resistance to sulfate wet–dry cycle erosion compared to SFRAC. According to the data in Table 12, the sulfate erosion resistance of the specimens decreases by 16.67%, 6.49%, and 10.19% at steel fiber dosages of 1%, 1.5%, and 2%, respectively. In contrast, when bamboo fibers are incorporated at dosages of 1%, 1.5%, and 2%, the sulfate erosion resistance of the specimens increases by 12.96%, 28.51%, and 9.72%, respectively.

6. Conclusions

In this paper, we systematically analyzed the changes in the apparent morphology, mass loss, relative dynamic elastic modulus, cubic compressive strength, and split tensile strength of recycled concrete specimens, including C, RAC, SFRAC, and BFRAC, through a coupled test of "dry and wet + sulfate erosion". We investigated the degradation characteristics of their mechanical properties and developed a durability degradation model based on the Weibull function to predict the specimens' service life. The following conclusions were drawn:

(1) After the specimens underwent standard maintenance, SFRAC developed yellow-brown rust stains due to the rusting of steel fibers in a high-humidity environment. After 30 dry–wet cycles, no significant changes were observed on the surface of the specimens except for the aggravation of rust on the SFRAC. After 60 cycles, the corrosion on the SFRAC intensified, and all specimens showed white frost on the surface. After 90 cycles, frost crystallization expanded on the surface, leading to cracks and a "skinning" phenomenon. After 120 cycles, the cracks expanded into a mesh, and mortar detachment occurred due to an increase in the number of holes. Beyond 120 cycles, the cracks formed a network, the mortar detached further, increasing the number of holes, and the corners of all specimens were damaged.

(2) Under the dry and wet cycles of sulfate erosion, the mass of each group of specimens initially increased and then decreased, reaching their maximum value at 45–60 cycles, and generally returning to their original mass by 105 cycles. In the early stages, sulfate penetrated into the specimen, increasing its mass, while in the later stages, intensified sulfate erosion caused the precipitation of cementitious materials, resulting in a decrease in mass. The quality change in RAC was more pronounced due to the high water absorption

of the recycled aggregate. Between 60 and 105 cycles, the specimen mass declined, but remained higher than the original mass. However, during the 105–120 cycle period, the mass dropped significantly due to mortar peeling and angular damage.

(3) The relative dynamic elastic modulus (RDM) of the specimens initially increased and then decreased under the sulfate wet and dry cycling conditions. The initial increase was attributed to the generation of C-S-H, which densified the concrete. The RAC exhibited a higher relative dynamic modulus due to the high number of internal cracks and the penetration of sulfate solution, which generated additional crystals. As the cycles progressed, the expansion stresses from calcite and gypsum crystallization, salt crystallization, and temperature-induced stresses caused damage to the concrete, leading to a decrease in the relative dynamic elastic modulus. After 120 cycles, the relative dynamic elastic modulus of bamboo fiber concrete was slightly higher than that of steel fiber concrete, with none of the specimens failing. SEM observations revealed that during the initial cycling phase (first 10 cycles), a large amount of dense C-S-H gel formed within the matrix, filling the initial pores. This phenomenon directly correlates with the initial increase in dynamic elastic modulus. In this study, the identification of halite and gypsum was based solely on morphological features observed in SEM images (e.g., needle-like crystals for gypsum and cubic crystals for halite), without phase verification techniques such as XRD or TG-DSC. Consequently, there exists a risk of misclassification of approximately 10–15%, particularly when the two products coexist or exhibit atypical crystalline morphologies. This study did not employ XRD or TG-DSC for direct phase verification; conclusions regarding morphological classification require comprehensive assessment in conjunction with chemical environment and elemental analysis. Future work will incorporate XRD phase analysis and synchrotron radiation CT technology to precisely identify the phase composition and spatial distribution of erosion products, thereby eliminating the risk of misclassification in morphological categorization.

(4) The compressive strength of each group of specimens initially increased and then decreased with the number of wet and dry cycles, reaching its maximum value at 45–60 cycles and largely recovering to its original state after about 90 cycles. The wet and dry cycles promote the secondary hydration of fly ash, which enhances the structural compactness. However, the formation of calcium alumina and gypsum leads to volume expansion, triggering microcracks and accelerating structural deterioration. After 120 wet and dry cycles, the corrosion resistance coefficient of compressive strength for steel fiber specimens was lower than that of RAC and decreased as the dosage increased. The bamboo fiber dosage of 1% was close to RAC but also decreased with an increase in dosage. (Advantages of a single fixed length: A fixed length eliminates the variability in bridging force caused by uneven fiber length distribution. This allows experimental results to more accurately reflect the inherent crack-inhibiting effect of the fiber type itself, rather than interference from length differences.)

(5) The split tensile strength and corrosion resistance coefficients of each group of specimens initially increased and then decreased with the number of wet and dry cycles, reaching their maximum values earlier for RAC and SFRAC (with high fiber content). The RAC exhibited more cracks due to the use of recycled aggregates, and the sulfate intrusion reaction generated products that filled the pore space, improving strength. In SFRAC, the steel fibers were slightly corroded at the initial stage, which made the specimens denser. After more than 90 wet and dry cycles, both the tensile strength and corrosion resistance coefficient decreased rapidly. When fiber content was less than 1.5%, it enhanced the tensile strength, which was higher than that of BFRAC, where accelerated loss occurred due to the characteristics of bamboo fibers. As a result, the tensile strength and corrosion resistance coefficient of BFRAC were higher than those of SFRAC.

(6) The reliability of each group of specimens, predicted using the Weibull function, indicates a longer expected lifespan of 290 wet and dry cycles for the 1.5% BFRAC specimens. This group shares identical mix proportions and curing conditions with other experimental groups, differing only in the absence of fibers. This ensures corrosion effects are solely determined by sulfate attack and the matrix's inherent properties, providing a reliable performance benchmark for fiber-reinforced groups.

(7) This research is based on accelerated testing environments; the applicability of its conclusions to natural long-term erosion scenarios requires further validation through field exposure tests. The weather resistance and long-term durability of bamboo fibers require extended follow-up studies. Future research may explore enhancing performance stability through methods such as coating modifications. The study considered only single sulfate corrosion; composite corrosion phenomena encountered in actual engineering applications (e.g., chloride-sulfate coupling) warrant further investigation.

Author Contributions: Methodology, C.Z. and J.Z.; Software, R.S. and S.W.; Validation, J.Z.; Resources, S.W.; Writing—original draft, S.W.; Writing—review and editing, R.S.; Project administration, C.Z.; Funding acquisition, C.Z. All authors have read and agreed to the published version of the manuscript.

Funding: This research was funded by the Knowledge Innovation Program of Wuhan-Shuguang Project (grant number 2023020201020375).

Data Availability Statement: The data presented in this study are available in the article. Further inquiries can be directed to the corresponding author.

Conflicts of Interest: Author Chuheng Zhong was employed by the company China Railway Major Bridge Engineering Group Co., Ltd. and author Shuai Wang was employed by the company Zhongcai India Chemical Building Material Private Limited. The remaining authors declare that the research was conducted in the absence of any commercial or financial relationships that could be construed as a potential conflict of interest.

References

1. Dzur, B.; Rother, W.; Nutsch, G.; Schilling, J.; Schwarze, A. Thermal Cutting of Concrete and RelatedMaterials[a]. *Ann. New York Acad. Sci.* **1999**, *891*, 223–230. [CrossRef]
2. Forero, J.; Brito, D.J.; Evangelista, L.; Pereira, C.H. Mechanical and fracture properties of concrete with recycled concrete aggregates treated with acids and addition of aluminium sulphate. *Constr. Build. Mater.* **2024**, *447*, 137947. [CrossRef]
3. Kim, J. Influence of quality of recycled aggregates on the mechanical properties of recycled aggregate concretes: An overview. *Constr. Build. Mater.* **2022**, *328*, 127071. [CrossRef]
4. He, X.S. Research on the effect of different fibers and contents on the mechanical properties of recycled concrete. *Sichuan Res. Build. Sci.* **2019**, *45*, 110–114.
5. Gu, S. *Basic Properties and Engineering Applications of Recycled Concrete*; Wuhan University Press: Wuhan, China, 2019.
6. Zega, C.J.; Di Maio, Á.A. Use of recycled fine aggregate in concretes with durable requirements. *Waste Manag.* **2011**, *31*, 2336–2340. [CrossRef]
7. Qin, S.S. *Study on Deterioration Model and Durability Failure of Sulfate-Eroded Concrete*; Harbin Institute of Technology: Harbin, China, 2020.
8. Yu, H.F.; Liu, L.X.; Cao, J.D.; Chen, H.Y.; Weng, Z.C. Durability and service life of concrete in chlorinated salt environments in east and west China. *J. Shenyang Univ. Archit. (Nat. Sci. Ed.)* **2005**, *21*, 125–129.
9. Wang, H.; Chen, Z.; Li, H.; Sun, X. Numerical simulation of external sulphate attack in concrete considering coupled chemo-diffusion-mechanical effect. *Constr. Build. Mater.* **2021**, *292*, 123325. [CrossRef]
10. Feng, P.; Bullard, J.W.; Garboczi, E.J.; Miao, C. A multiscale microstructure model of cement paste sulfate attack by crystallization pressure. *Model. Simul. Mater. Sci. Eng.* **2017**, *25*, 065013. [CrossRef]
11. Zhang, H.; Ji, T.; Liu, H. Performance evolution of the interfacial transition zone (ITZ) in recycled aggregate concrete under external sulfate attacks and dry-wet cycling. *Constr. Build. Mater.* **2019**, *229*, 116938. [CrossRef]
12. Xie, F.; Li, J.; Zhao, G.; Zhou, P.; Zheng, H. Experimental study on performance of cast-in-situ recycled aggregate concrete under different sulfate attack exposures. *Constr. Build. Mater.* **2020**, *253*, 119144. [CrossRef]

13. Feng, P.; Garboczi, J.E.; Miao, C.; Bullard, J.W. Microstructural origins of cement paste degradation by external sulfate attack. *Constr. Build. Mater.* **2015**, *96*, 391–403. [CrossRef]
14. Mehta, P.K. Mechanism of expansion associated with ettringite formation. *Cem. Concr. Res.* **1973**, *3*, 1–6. [CrossRef]
15. Xie, B.Y. *Research on Sulfate Erosion Resistance of Recycled Aggregate Concrete*; Huazhong University of Science and Technology: Wuhan, China, 2014.
16. Kumarasamy, K.; Karthikeyan, K.; Shyamala, G.; Gebreyowhanse, H. Strength Properties of Bamboo Fiber Reinforced Concrete. *IOP Conf. Ser. Mater. Sci. Eng.* **2020**, *981*, 032063. [CrossRef]
17. Wen, S.T.; Xu, R.T.; Sun, K.; Lu, T.H.; Wei, R.Z.; Lu, X.C. Effects of heat treatment on the structure and mechanical properties of bamboo. *Biomass Chem. Eng.* **2024**, *58*, 53–59.
18. Zhong, C.; Wang, D.; Zhang, L.; Mao, W.; Xing, S.; Chen, J.; Xiao, Y. Durability analysis of metakaolin recycled concrete under sulphate dry and wet cycle. *Sci. Rep.* **2024**, *14*, 16435. [CrossRef]
19. *GB/T 50081-2002*; Standard for Test Method of Mechanical Properties on Ordinary Concrete. Chinese Standard. Chinese Building Press: Beijing, China, 2002.
20. *GB/T 50082-2009*; Test Method Standard for Long-term Performance and Durability of Ordinary Concrete. China Architecture and Building Press: Beijing, China, 2009.
21. Gu, R.; Wang, J.; Li, B.; Qi, D.; Gao, X.; Yang, Z. Experimental Study on Mechanical Properties and Compressive Constitutive Model of Recycled Concrete under Sulfate Attack Considering the Effects of Multiple Factors. *Buildings* **2024**, *14*, 2761. [CrossRef]
22. Quan, X.Y. *Research on Durability of Fiber Concrete Under Sulfate Dry and Wet Environment*; Xijing College: Xi'an, China, 2020. [CrossRef]
23. Wang, Z.B.; Sun, P.; Liu, W.K.; Han, Y.D. Mechanical properties and microstructure of ECC axial tensile under sulfate attack. *J. Huazhong Univ. Sci. Technol. (Nat. Sci. Ed.)* **2021**, *49*, 31–36.
24. Liu, Z.Q.; Deng, D.H.; De Schutter, G.; Liu, Y.H. Microanalysis of sulfate crystallization damage in concrete(I)-cement mortar. *J. Silic.* **2012**, *40*, 186–193. [CrossRef]
25. Zhang, S.Y. *Research on Physical and Mechanical Properties and Durability of Nano-Metakaolin Cementitious Materials*; Dalian Maritime University: Dalian, China, 2017.
26. Bai, Y.H.; Yu, S.; Chen, W. Research on sulfate erosion resistance of alkali slag concrete. *Funct. Mater.* **2017**, 43–46.
27. Haufe, J.; Vollpracht, A. Tensile strength of concrete exposed to sulfate attack. *Cem. Concr. Res.* **2019**, *116*, 81–88. [CrossRef]
28. Bai, W.; Suo, G.; Yuan, C.; Guan, J.; Xie, C.; Li, L. Study on multi-scale dynamic mechanical properties of metakaolin modified recycled aggregate concrete under coupling conditions of sulfate attack and dry-wet cycles. *J. Build. Eng.* **2024**, *94*, 109921. [CrossRef]
29. Wang, Y.N.; Pei, Q. Research progress of fiber reinforced cementitious materials from agricultural waste. *J. Guangdong Inst. Petrochem. Technol.* **2023**, *33*, 70–73+81.
30. He, H.T. Experimental study on mechanical properties of plant fiber reinforced concrete. *Synth. Fiber* **2024**, *53*, 54–59. [CrossRef]
31. Min, D.D.; Jiang, X.Y. Research on the enhancement effect of natural bamboo fiber materials on the mechanical properties of general concrete. *Pap. Sci. Technol.* **2024**, *43*, 86–88+61.
32. Xiao, H.Q.; Cao, Y.Z.; Guan, X.; Li, Q.; Liu, X.L. Damage to recycled concrete with different aggregate substitution rates from the coupled action of freeze-thaw cycles and sulfate attack. *Constr. Build. Mater.* **2019**, *221*, 74–83. [CrossRef]

Disclaimer/Publisher's Note: The statements, opinions and data contained in all publications are solely those of the individual author(s) and contributor(s) and not of MDPI and/or the editor(s). MDPI and/or the editor(s) disclaim responsibility for any injury to people or property resulting from any ideas, methods, instructions or products referred to in the content.